JMEPEG (2007) 16:766–774
DOI: 10.1007/s11665-007-9094-3

©ASM International
1059-9495/$19.00

Stress Variation in Deep Drawn 1017 Aluminum Alloy

S.A. Balogun, S.O. Adeosun, and D.E. Esezobor

(Submitted September 6, 2006; in revised form October 7, 2006)

The qualitative analysis of the elastic-plastic behavior of metal sheet is usually performed by finite element methods. These methods are often complicated because of large computational requirements associated with the use of realistic models. In this paper, an effective model based on the macro-mechanical properties of the metal blank and tool geometry is used to describe the anisotropic plastic flow of the metal sheet in plane stress condition. The model is derived from the fundamental deflection equation of beam/column. The model used to optimize the stamping process is designed to be as close to realistic forming conditions as possible.

Keywords aluminum sheet, beam/column, deep drawn, elastic-plastic, model, stress-strain

1. Introduction

The problem of optimal blank shape design for the cup forming process has attracted the attention of researchers. A good number of works to characterize anisotropy of sheet metal with useful yield function for plastic flow have been carried out. For workhardening of metals empirical and semi-empirical formulas for one-dimensional case have been presented (Ref 1-10). The power law, which is applicable to stretch formability, does not account for any strain rate or temperature effects. The Johnson-Cook is often used in finite element codes to introduce strain rate and temperature dependence of the flow stress. Its accuracy of the curve fitting to experimental data is not satisfactory for most materials. The Voce model fits experimental data and accounts for the saturation of flow stress at relatively large strains. However, it is not equally accurate in the whole range of strains.

The earing defect in formed cup is a result of planar anisotropy in the rolled sheet. This variation of material properties along different directions of the rolled sheet occurs during thermo-mechanical processing of the sheet before drawing is done. Barlat et al. (Ref 1) predicted earing in polycrystals with a model in which the flange was analyzed. It was found out that plane strain assumption successfully explained the major trends of earing. The work of Becker et al. (Ref 2) on single crystals agrees with that of Barlat et al. (Ref 1, 2).

Although the analysis of the elastic-plastic behavior of crystalline solids is of great importance for fundamental and practical reasons, qualitative analyses by finite element methods are often complicated by the large computational requirements associated with the use of realistic models (Ref 3).

A large volume of research has been dedicated to characterizing anisotropy of sheet metal and to develop a useful yield function for plastic flow. The quadratic anisotropic yield criterion of Hill (Ref 4) has been widely used. This model predicts the behavior of certain metals including some aluminum alloys. There are a number of nonquadratic yield criteria, which were developed by Gotoh (Ref 5), Bassani (Ref 6), and Logan and Hosford (Ref 7). These were found ineffective for modeling planar anisotropy in sheet metal under general loading conditions. For plane stress conditions Barlat and Lian (Ref 8) proposed a nonquadratic planar anisotropic yield function where three parameters describe the anisotropy in the sheet metal. Barlat and Lege (Ref 9) proposed a six-component model for planar anisotropy in sheet metal applicable to three-dimensional deformations. Chung and Shah (Ref 10) demonstrated the effectiveness of this model in the finite element simulation of sheet metal forming. Pegada et al. (Ref 11) have proposed an effective algorithm for the determination of optimal blank shape for cups using the planar anisotropic function proposed by Barlat et al. (Ref 9). The algorithm uses an iterative process to arrive at the optimum blank shape.

In this paper, an effective model based on the macro-mechanical properties of the sheet and tool geometry is used to describe the anisotropic plastic flow of the sheet metals in plane stress condition.

2. Methodology

2.1 Theoretical Analysis

The cup forming process involves placing a well lubricated circular blank sheet on a die, which is held down by a blank holder and the punch, P moves with the sheet through the die opening. The punch is withdrawn when the required cup height is attained. For this analysis the formed cup has been taken to consist of three sections namely AB, BC, and CD (Fig. 1). Sections AB and BC are treated as beams having uniform cross sections, while CD is taken to be a column.

S.A. Balogun, S.O. Adeosun, and **D.E. Esezobor,** Department of Metallurgical and Materials Engineering, University of Lagos, Akoka-Yaba, Lagos, Nigeria. Contact e-mail: esezobordave@yahoo.com.

Case 1 Elastic Deformation (Section *AB*)

For the case of elastic deformation, Section *AB* is taken to be a beam of length *l*.

Consider a beam *AB* of length *l* fixed at one end and carrying a load *P* uniformly distributed over its entire length, the magnitude of the load per unit length (the load intensity) being *q* (Fig. 2).

The sum of all forces lying to the left of section M_n is $Q = -qx$. (Eq 1)

The maximum shear force Q_{max} occurs at the fixed support and is given as $Q_{max} = -P$.

Considering the left-hand cut-off part, we obtain the bending moment as

$$M = -qx\frac{x}{2} = -q\frac{x^2}{2}. \quad \text{(Eq 2)}$$

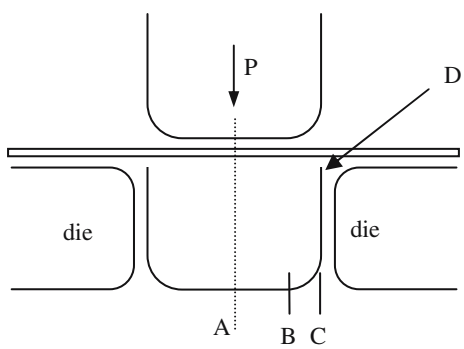

Fig. 1 Schematic of drawing operation before and after drawing

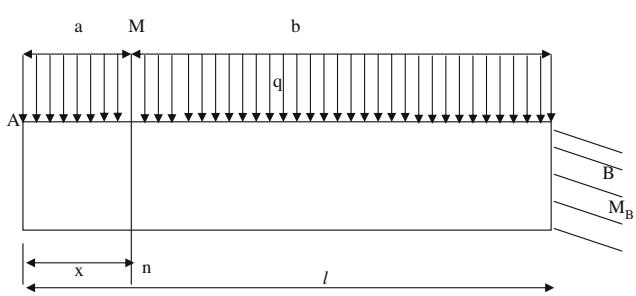

Fig. 2 Section *AB* under elastic deformation

The maximum moment Q_{max} occurs at the fixed support, where $x = l$ and is given as

$$M_{max} = -q\frac{l^2}{2} = -P\frac{l}{2}.$$

Comparing this moment with the maximum bending moment in the case of a concentrated force applied at the center of the beam, we see that the maximum bending moment for a uniformly distributed load is half the value for a concentrated force. It should be noted that $Q = dM/dx$ and $q = d^2M/dx^2$,

The general equation of the elastic curve is given by

$$M = El\frac{d^2y}{dx^2}. \quad \text{(Eq 3)}$$

Deflection y at mid-length where $x = l/2$ is given as

$$y = -p\frac{l^3}{384El}. \quad \text{(Eq 4)}$$

But bending stress formula provides that $\frac{\sigma}{y} = \frac{M}{I} = \frac{E}{R}$, where y is the vertical deflection of beam, σ the bending stress, E the Young's modulus of elasticity of material, I the moment of inertia, R the radius of curvature or punch corner radius.

The bending stress on section *AB* of the cup is therefore expressed as

$$\sigma_{x=\frac{l}{2}} = \frac{P^2l^4}{3072El^2}. \quad \text{(Eq 5)}$$

Case 2 Elastic-Plastic Transition

In the elastic-plastic transition region (section *BC*), the entire plastic region starts in this very small area. Here the deformation is largely plastic. Enlarged form of *BC* is shown in Fig. 3. *P* can be resolved into forces S_x,S_y.

During deformation, section *BC* becomes oblique. The stresses acting on the oblique plane are the normal stress σ and the shear stress τ.

Let the normal to this plane (*BC*) be the x^1 direction and direction lying in the oblique plane be the y^1 direction.

The assumptions for this description are that the plane is at infinitesimal distance from 0 and the element is so small that variations in stress over the sides of the element can be neglected.

The normal and shear stresses acting on the oblique plane are given as

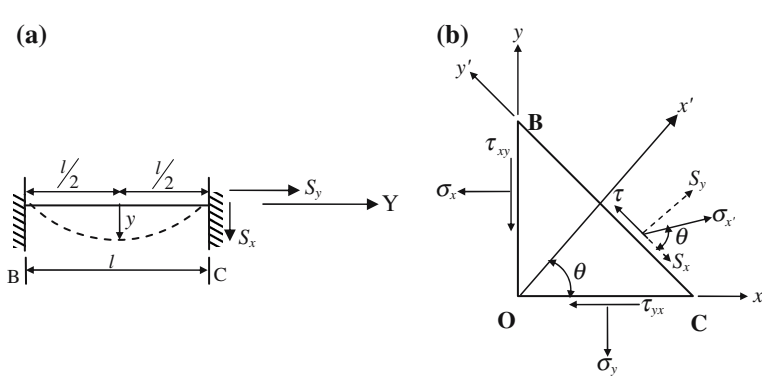

Fig. 3 Cup corner region in horizontal plane (a) and oblique plane (b)

$$\sigma_{x^1} = S_x \cos\theta + S_y \sin\theta \Rightarrow$$
$$\sigma_{x^1} = \sigma_x \cos^2\theta + \sigma_y \sin^2\theta + 2\tau_{xy}\sin\theta\cos\theta \quad \text{(Eq 6)}$$

$$\tau_{x^1y^1} = S_y \cos\theta - S_x \sin\theta \Rightarrow$$
$$\tau_{x^1y^1} = \tau_{xy}(\cos^2\theta - \sin^2\theta) + (\sigma_y - \sigma_x)\sin\theta\cos\theta. \quad \text{(Eq 7)}$$

To determine σ_{y^1} put $(\theta + \frac{\pi}{2})$ in place of θ in Eq 6. Since σ_{y^1} is orthogonal to σ_{x^1}

$$\sigma_{y^1} = \sigma_x \cos^2\left(\theta + \frac{\pi}{2}\right) + \sigma_y \sin^2\left(\theta + \frac{\pi}{2}\right) + 2\tau_{xy}\sin\left(\theta + \frac{\pi}{2}\right)\cos\left(\theta + \frac{\pi}{2}\right), \text{ that is,}$$
$$\sigma_{y^1} = \sigma_x \sin^2\theta + \sigma_y \cos^2\theta - 2\tau_{xy}\sin\theta\cos\theta. \quad \text{(Eq 8)}$$

Bending moment at any section of the bar (Fig. 3a) is

$$M = Py. \quad \text{(Eq 9)}$$

2.2 Euler's Formula

Assume that the deflected axis or the elastic curve of section *BC* represents a sine curve. Let the magnitude of the deflection at the middle of the bar be *f*.

The elastic curve equation is then

$$y = f \sin\frac{\pi x}{l}, \quad \text{(Eq 10)}$$

when there is no deflection, $y = 0$. At points *B* and *C*, $x = 0$ and $x = l$, respectively.

At the middle of the bar i.e. at $x = l/2$, the deflection is equal to *f* and $dy/dx = 0$.

$$\Rightarrow M = Pf \sin\frac{\pi x}{l}. \quad \text{(Eq 11)}$$

The bending stresses in x^1 and y^1 axes are $\sigma_{x'} = \frac{Py}{(y^2+R^2)^{\frac{1}{2}}}\left[\cos\theta - \frac{R}{y}\sin\theta\right]$ and $\sigma_{y^1} = \frac{-Py}{(y^2+R^2)^{\frac{1}{2}}}\sin\theta + \frac{-PR}{(y^2+R^2)^{\frac{1}{2}}} \times \cos\theta = -\frac{Py}{(y^2+R^2)^{\frac{1}{2}}}\left[\sin\theta + \frac{R}{y}\cos\theta\right]$.

The shear stress is given as

$$\tau_{x^1y^1} = S_y\cos\theta - S_x\sin\theta = \frac{-PR}{(y^2+R^2)^{\frac{1}{2}}}\cos\theta - \frac{-Py}{(y^2+R^2)^{\frac{1}{2}}}\sin\theta$$
$$\tau_{x^1y^1} = -\frac{Py}{(y^2+R^2)^{\frac{1}{2}}}\left[\frac{R}{y}\cos\theta + \sin\theta\right]. \quad \text{(Eq 12)}$$

Case 3 Plastic Deformation (section *CD*)

Consider section *CD* as a column with end *C* built in and end *D* hinged. This section experiences bending and unbending stresses.

The stresses acting at *C* are $\sigma_{x^1}, \sigma_{y^1}$ and $\tau_{x^1y^1}$ due to the stress on the oblique plane *BC*. For a column with both ends hinged, the equilibrium equation is

$$EI\frac{d^2y}{dx^2} + Py = 0. \quad \text{(Eq 13)}$$

This equation follows from the condition that the sum of the bending moments at any section is zero. It assumes this simple form because shear forces and moments at the end supports do not exist. For other end conditions, there will be in general an unknown shear and bending moment acting at the end support, and the equilibrium equation will be of the form

$$EI\frac{d^2y}{dx^2} + Py = Qx + M_0, \quad \text{(Eq 14)}$$

where Q is the shear force and M_0 is the bending moment at the end of the column.

Using Eq 14 as the starting equilibrium equation and differentiating with respect to x twice, we have

$$\frac{d^2}{dx^2}\left(EI\frac{d^2y}{dx^2}\right) + P\frac{d^2y}{dx^2} = 0. \quad \text{(Eq 15)}$$

Equation 15 is the differential equation of equilibrium for a column with any boundary condition. It expresses the condition that the sum of shear forces on an element of the column is zero. For columns with constant cross sections made of homogeneous material, EI is independent of x and Eq 15 becomes

$$\frac{d^4y}{dx^4} + K^2\frac{d^2y}{dx^2} = 0, \quad \text{(Eq 16)}$$

where $K^2 = P/EI$. Equation 16 is an ordinary differential equation with constant coefficients. The general solution will be

$$y = C_1 \sin Kx + C_2Kx + C_3x + C_4, \quad \text{(Eq 17)}$$

where C_1, C_2, C_3, and C_4 are constants.

For a column with one end built in and the other end hinged, the boundary conditions are that, at

$$x = 0, \quad y = 0 \quad \text{and} \quad \frac{dy}{dx} = 0;$$
$$\text{and at } x = l, \quad y = 0 \quad \text{and} \quad \frac{d^2y}{dx^2} = 0.$$

Thus for section *CD* the bending and shear stresses are, respectively,

$$\sigma_{x^1} = \frac{P}{(y^2+l^2)^{\frac{1}{2}}}[l\cos\theta - y\sin\theta]. \quad \text{(Eq 18)}$$

$$\tau_{x^1y^1} = -\frac{p}{(y^2+l^2)^{\frac{1}{2}}}[y\cos\theta + l\sin\theta]. \quad \text{(Eq 19)}$$

Since σ_{y^1} is orthogonal to σ_{x^1}, replace θ with $(\theta + \frac{\pi}{2})$ to determine σ_{y^1}.

$$\sigma_{y^1} = -\frac{p}{(y^2+l^2)^{\frac{1}{2}}}[l\sin\theta + y\cos\theta]. \quad \text{(Eq 20)}$$

The stresses acting on *CD* of the formed cup are taken as principal stresses and may be summarized as follows:

$$\sigma_1 = \frac{P}{(2\bar{\varepsilon})^{\frac{1}{2}}}[(1+\bar{\varepsilon})\theta\cos\theta - \bar{\varepsilon}\sin\theta] \quad \text{(Eq 21)}$$

$$\sigma_2 = -\frac{P}{(2\bar{\varepsilon})^{\frac{1}{2}}}[(1+\bar{\varepsilon})\theta\sin\theta + \bar{\varepsilon}\cos\theta] \quad \text{(Eq 22)}$$

$$\tau_{x'y'} = -\frac{P}{(2\bar{\varepsilon})^{\frac{1}{2}}}[\bar{\varepsilon}\cos\theta + (1+\bar{\varepsilon})\theta\sin\theta]. \quad \text{(Eq 23)}$$

These equations are functions of P, R, ε and θ.

The deviatoric strain-increment is defined as $d\varepsilon_{ij}^{1} = d\varepsilon_{ij} - \varepsilon_{ij}d\varepsilon$ and $d\varepsilon = \frac{1}{3}d\varepsilon_{ii}$. However, $d\varepsilon = \frac{(1-2\nu)}{E}d\sigma$ and $d\varepsilon_{ij}^{l} = d\varepsilon_{ij}^{p} + \frac{d\sigma_{ij}^{i}}{2G}$ where $d\varepsilon$ is the effective strain.

If we consider yielding under uniaxial tension,

$$\sigma_{xa} = \sigma_1 \neq 0, \quad \sigma_2 = \sigma_3 = 0, \quad \text{and } \sigma_m = \frac{\sigma_1}{3}.$$

Since only the deviatoric stresses cause yielding,

$$\sigma_1^1 = \sigma_1 - \sigma_m = 2\frac{\sigma_1}{3}, \sigma_2^1 = \sigma_3^1 = -\frac{\sigma_1}{3},$$

from which we find $\sigma_1^1 = -2\sigma_2^1 = -2\sigma_3^1$.

From the condition of constancy of volume in plastic deformation

$$d\varepsilon_1 = -2d\varepsilon_2 = -2d\varepsilon_3, \quad \text{so that } \frac{d\varepsilon_1}{d\varepsilon_2} = -2 = \frac{\sigma_1^1}{\sigma_2^1}.$$

The effective stress or equivalent stress $\bar{\sigma}$ is given as

$$\bar{\sigma} = \frac{\sqrt{2}}{2}\left[(\sigma_1 - \sigma_2)^2 + (\sigma_2 - \sigma_3)^2 + (\sigma_3 - \sigma_1)^2\right]^{\frac{1}{2}} = F(W_P) = Y = \sqrt{3K}. \quad \text{(Eq 24)}$$

2.3 Total Plastic Strain

If the straining is proportional (with a constant ratio of $d\varepsilon_1 : d\varepsilon_2 : d\varepsilon_3$), the total plastic strain may be expressed in terms of the total strains as $\bar{\varepsilon} = \left[\frac{2}{3}\left(\varepsilon_1^2 + \varepsilon_2^2 + \varepsilon_3^2\right)\right]^{\frac{1}{2}}$. But $\varepsilon_2 = \varepsilon_{y_1}, \varepsilon_3 = -\upsilon\varepsilon_y = -\upsilon\varepsilon_2$, where υ is the Poisson's ratio.

Thus,

$$\bar{\varepsilon} = \frac{PR^2\theta^3}{384EI}\left[\frac{2}{3}\left(2\upsilon^2 + 1\right)\right]^{1/2}, \quad \text{(Eq 25)}$$

where θ is in radians

Effective stress,

$$\bar{\sigma} = \frac{P\left[2(1+\bar{\varepsilon})^2\theta^2 + 2\bar{\varepsilon}^2 + (1+\bar{\varepsilon})^2\theta^2\sin 2\theta - \bar{\varepsilon}^2\sin 2\theta\right]^{\frac{1}{2}}}{2(\bar{\varepsilon})^{\frac{1}{2}}} \quad \text{(Eq 26)}$$

Effective strain,

$$d\bar{\varepsilon} = \frac{P\left[2(1+\varepsilon)^2\theta^2 + 2\bar{\varepsilon}^2 + (1+\bar{\varepsilon})^2\theta^2\sin 2\theta - \bar{\varepsilon}^2\sin 2\theta\right]^{\frac{1}{2}}d\lambda}{3(\bar{\varepsilon})^{\frac{1}{2}}} \quad \text{(Eq 27)}$$

2.4 Stress and Strain Models

The equations in section *CD* above are for an isotropic material. The heterogeneous nature of the sheet and the degree of deformation affect the hardness and Young's modulus, *E* of the material. The orientation of the grains in relation to the rolling direction denoted as (θ) is influenced by the heterogeneous nature of the material. The parameter *k*, which defines the dislocation density through the sheet, depends on the intensity of plastic work carried out. If the degree of deformation is denoted as γ, for anisotropic material, the isotropic model equations will be represented as follows.

2.5 Strain Model

The empirical strain model is given below

Effective strain,

$$d\varepsilon = \frac{P[(1+\varepsilon)^2\theta^2(2+\sin 2\theta) + \varepsilon^2(2-\sin 2\theta)]^{\frac{1}{2}}d\lambda}{3(\varepsilon)^{\frac{1}{2}}}. \quad \text{(Eq 28)}$$

2.6 Plastic Strain

$$\text{Total plastic strain, } \varepsilon = \frac{KPR^2\theta^3\left[\frac{2}{3}(2\upsilon^2+1)\right]^{\frac{1}{2}}}{384EI}. \quad \text{(Eq 29)}$$

2.7 Stress Model

Effective stress,

$$\sigma = \frac{P\gamma[(1+\varepsilon)^2\theta^2(2+\sin 2\theta) + \varepsilon^2(2-\sin 2\theta)]^{\frac{1}{2}}}{2a(\varepsilon)^{\frac{1}{2}}} \quad \text{(Eq 30)}$$

where *R* is the forming tool parameter (punch corner radius), m; θ the inclination of test sample to the rolling direction in radian; *P* the punch force, N; *a* the cross-sectional area of test piece, m^2; *E* the Young modulus of material; *I* the moment of inertia of material; *K* the dislocation density, m^{-2}; γ the degree of deformation; υ Poisson ratio $\approx$ 0.36 (0.33-0.55); $d\lambda$ the ratio of plastic strain increment to deviatoric stress = 0.001.

3. Experimental Analysis

Materials and test facilities for experimentation were provided by Aluminum Rolling Mills, Ota Ogun State, Nigeria. Cold and hot rolled aluminum sheets that have been annealed were used for the experimental and theoretical analyses of stress variation in cup forming.

Test samples were made from 1.2 and 1.6 mm thickness of both cold and hot rolled sheet. The thickness and chemical composition of these sheets are shown in Table 1.

Experimental tests were carried out through the following routes.

3.1 Tensile Test

Rectangular test pieces of greater dimension than required for tensile test were cut from a circular blank sheet—using snip

Table 1 Chemical composition of specimens

Sheet thickness, mm	Al	Fe	Si	Cu	Mg	Material processing condition
1.2	99.38	0.31857	0.09316	0.13057	<0.00187	Cold rolled
1.6	99.01	0.51155	0.22595	0.04443	0.002	
1.2	99.54	0.25600	0.09237	0.00685	0.001	Hot rolled
1.6	99.53	0.2756	0.09912	0.00754	0.00116	

Quality level: Fe ≤ 0.4%, Cu ≤ 0.05, Si ≤ 0.23%

after geometrical markings have been done at various angles to the rolling direction. These were placed on a die with a cylindrical cavity and blanked by a manually operated machine. Two flat tensile pieces of the form shown in Fig. 4 were prepared for each of the sheet thickness at angles 0°, 45° and 90° to the rolling direction. The test sample was gripped between the ends of the tensometer-testing machine and axis of tension is along the axis of the test sample. A maximum test load of 5 kN was used during the experiment.

Thickness of test piece = t, gauge length $(l_0) = 50 \pm 0.5$ mm, total length $(l_T) = 100$ mm, final length is (l_f) mm. The results of a tensile test may be expressed as:

$$\text{Tensile strength} = \frac{\text{maximum load}}{\text{original cross-sectional area}}$$

$$\text{Similarly, \% elongation} = \frac{\text{increase in gauge length}}{\text{original gauge length}} \times 100 = \frac{l_f - l_0}{l_0} \times 100.$$

4. Results

4.1 Experimental Empirical Relations and Theoretical Model

Several empirical formulae have been proposed for fitting stress-strain curves. In many metals the (σ, ε) curve has an approximately constant slope at very large strains. The curve for such a metal, when heavily prestrained, is closely represented by $\sigma = a + b\varepsilon$.

In some metals a more successful formula for moderate strains is $\sigma = a + (b - a)(1 - e^{-c\varepsilon})$, where e denotes the exponential constant. Voce and Palm proposed this independently. However, for very small or purely elastic strains the formula fails.

4.2 Theoretical and Experimental Relations

Using regression analysis to fit a curve to the experimental stress-strain results; a quadratic relation of the form $\sigma = a + b\varepsilon + c\varepsilon^2$ fits well with the data having r^2 values ranging from $0.92 < r^2 \leq 0.99$. The stress-strain curves are displayed in Fig. 5-16.

Generally, at $\theta = 0°, 45°$ and $90°$, quadratic empirical relations of the form $\sigma = a + b\varepsilon + c\varepsilon^2$ fit well with the experimental data and are in close agreement with the theoretical model developed for stress variation in cup forming.

In Fig. 5 and 6 there is a close agreement between theory and experiment in the strain range $0 < \varepsilon < 0.5$. In Fig. 8, the agreement exists in strain range $0 \leq \varepsilon \leq 1.6$. From Fig. 7, 9-16 there is a good agreement between the theory and experiment in

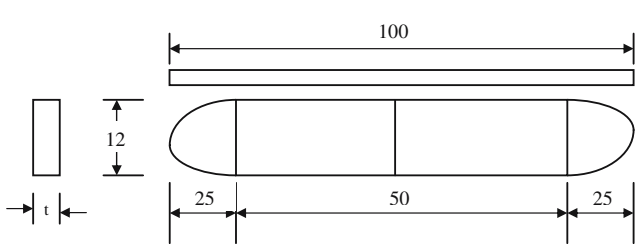

Fig. 4 Tensile test piece sample (dimensions in mm)

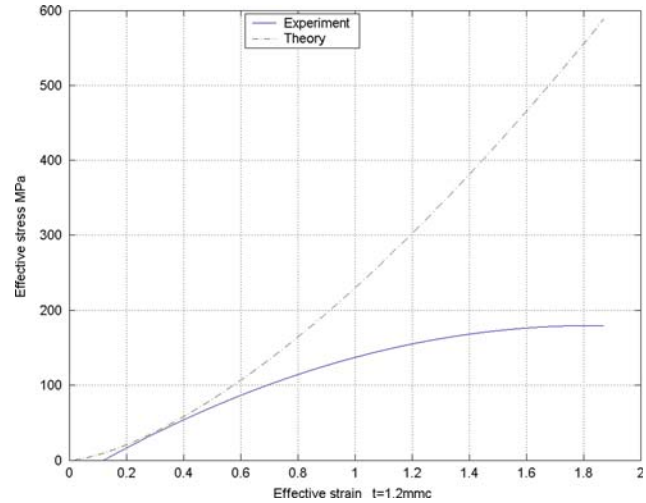

Fig. 5 Graph of effective stress vs. effective strain (experiment/theory) at 0° to rolling direction

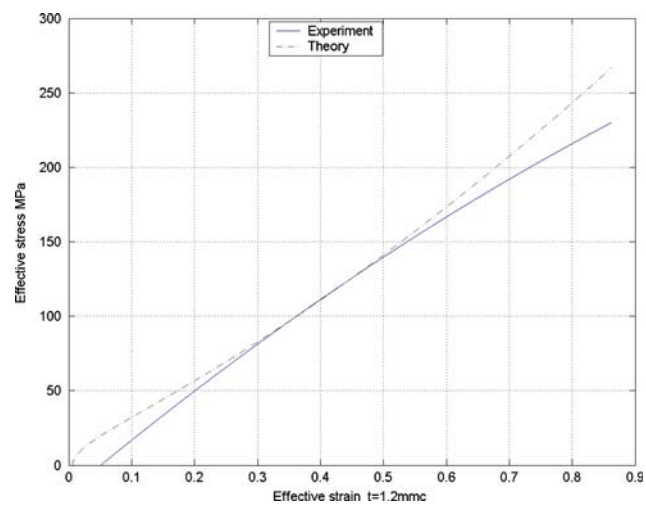

Fig. 6 Graph of effective stress vs. effective strain (experiment and theory) at 45° to rolling direction

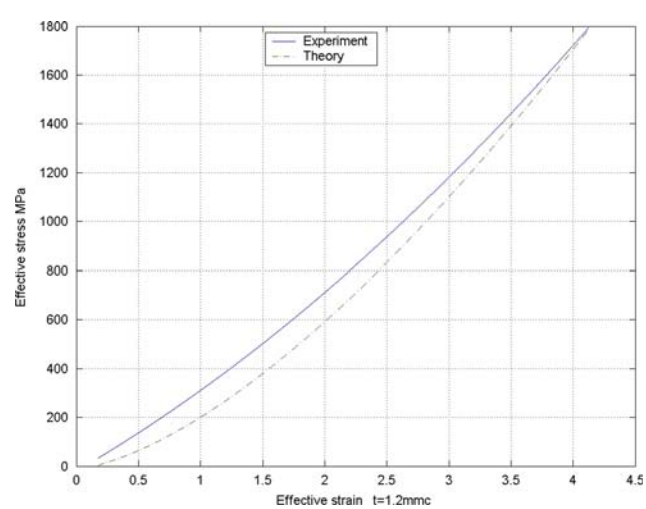

Fig. 7 Graph of effective stress vs. effective strain (experiment and theory) at 90° to rolling direction

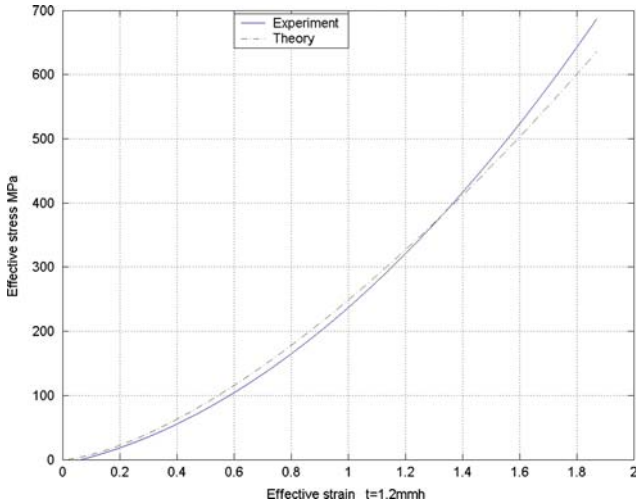

Fig. 8 Graph of effective stress vs. effective strain (experiment and theory) at 0° to rolling direction

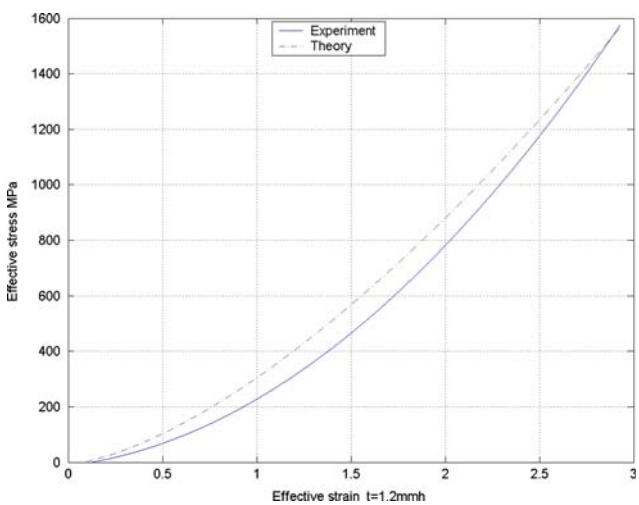

Fig. 9 Graph of effective stress vs. effective strain (experiment and theory) at 45° to rolling direction

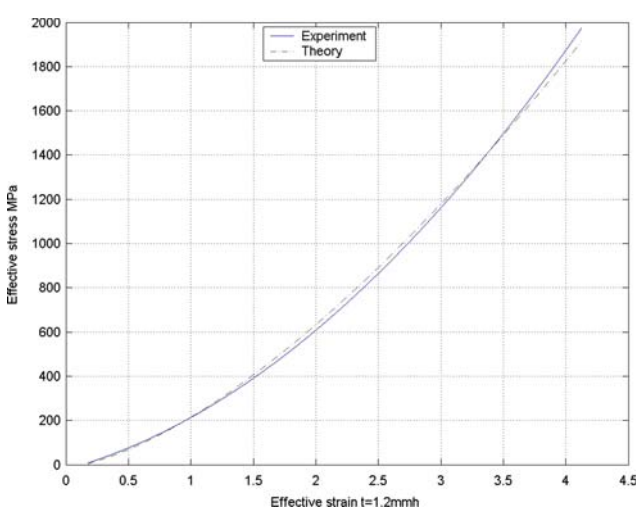

Fig. 10 Graph of effective stress vs. effective strain (experiment and theory) at 90° to rolling direction

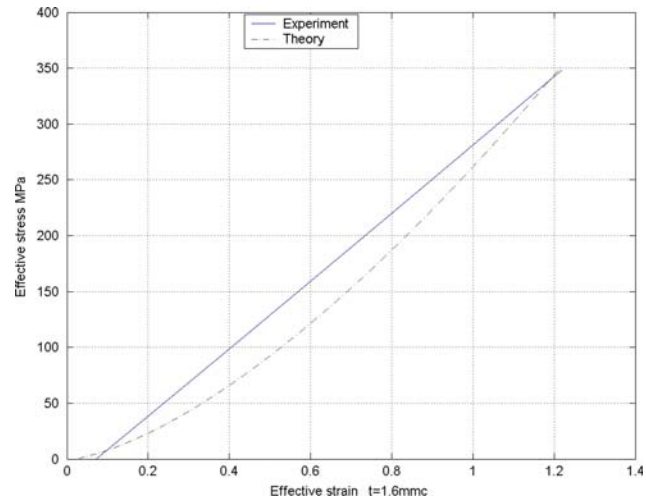

Fig. 11 Graph of effective stress vs. effective strain (experiment and theory) at 0° to rolling direction

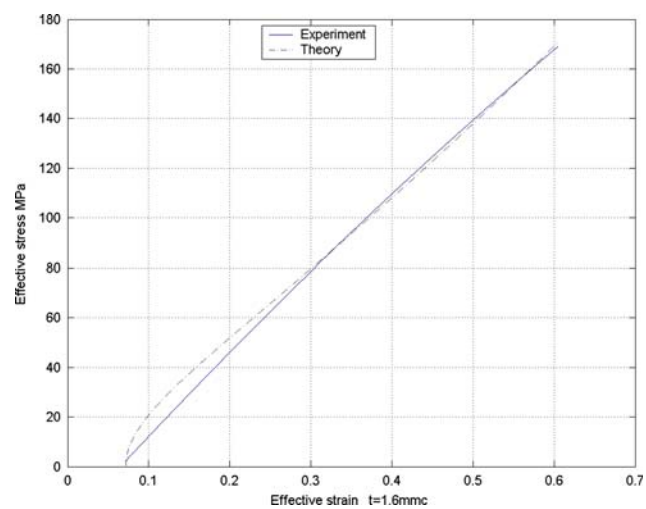

Fig. 12 Graph of effective stress vs. effective strain (experiment and theory) at 45° to rolling direction

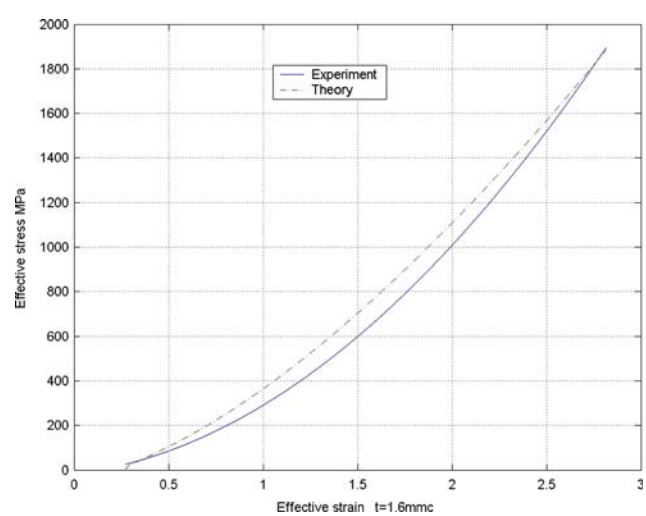

Fig. 13 Graph of effective stress vs. effective strain (experiment and theory) at 90° to rolling direction

the strain range considered. The anisotropic stress variations between the theory and experiment are shown in Table 2.

The above results indicate the variation from the rolling direction of anisotropic behavior of plastic flow towards the direction normal to rolling direction. The ultimate stresses occur at normal to the rolling direction independent of the sheet rolling temperature. The stresses observed in the various directions show that hot rolled sheet flow plastically more readily than cold rolled sheet. However, it should be noted that if particles of troublesome elements like copper and iron are above the quality level prescribed for practical work, the precipitation of these elements in the rolling direction will not significantly affect the flow stress. At normal to rolling direction the presence of the precipitates of copper and iron will increase the flow stress in this region appreciably.

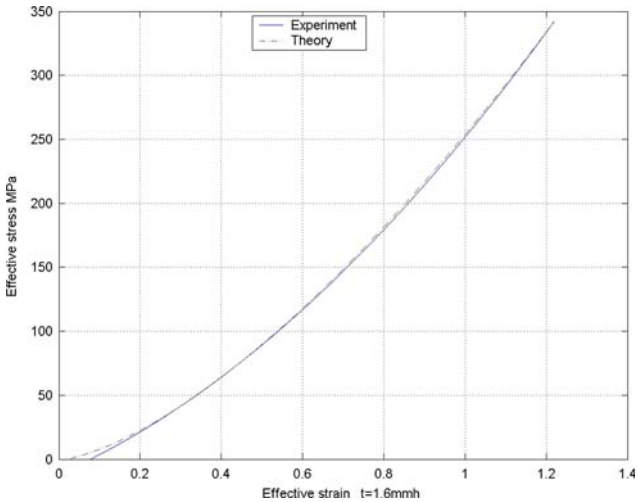

Fig. 14 Graph of effective stress vs. effective strain (experiment and theory) at 0° to rolling direction

4.3 Dislocation Density

The derived plastic strain relation (Eq 29) is a function of dislocation density for an anisotropic material. This plastic strain is fitted into both the stress model and the empirical relation obtained from experimental data. The resultant stress obtained in both cases was compared to determine the dislocation density value. Dislocation density is highest in the rolling direction and independent of both the thickness and the rolling temperature of sheet (Table 3). The least dislocation density occurs at 90° to the rolling direction, an indication of low resistance to deformation. The above show that there is property variation from the rolling direction outwards. It should be noted that annealing after cold working of the material produces dislocation density in the neighborhood of 10^2 mm^{-2}. The cause of this occurrence may be the prompt recovery for crystals perpendicular to the rolling direction as a result of the formation of new equiaxed crystals, while no full recovery is achieved for those crystals along the rolling direction. It may also be that along the rolling direction, crystals with different

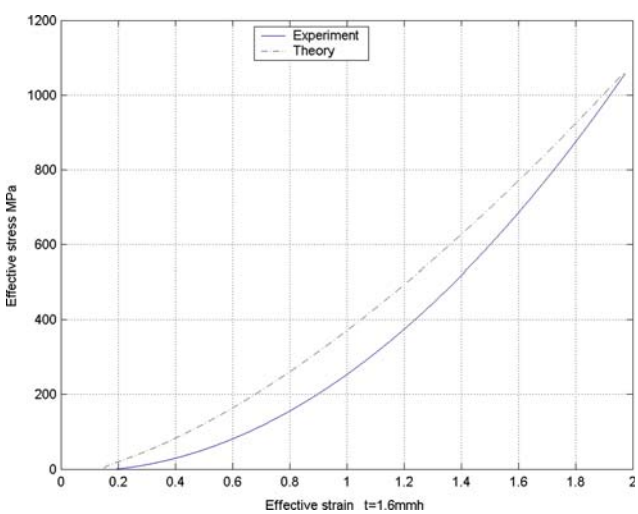

Fig. 15 Graph of effective stress vs. effective strain (experiment and theory) at 45° to rolling direction

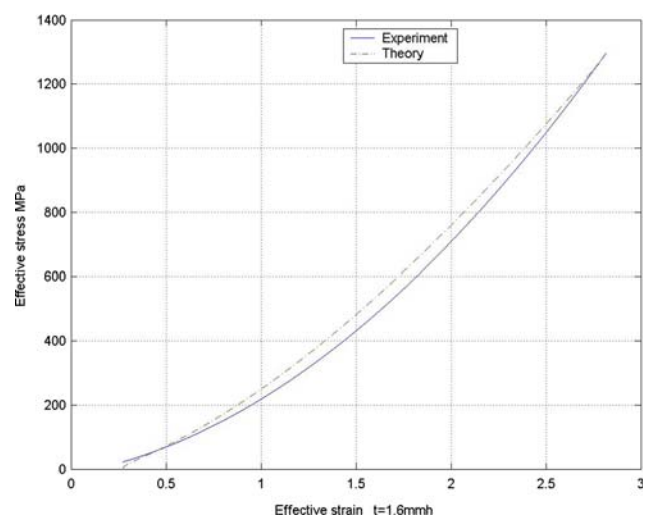

Fig. 16 Graph of effective stress vs. effective strain (experiment and theory) at 90° to rolling direction

Table 2 Values of ultimate stress for some 1017 Aluminum sheets (theory and experiment)

		Ultimate stress, MPa with inclination to the rolling direction					
		0°		45°		90°	
Sheet thickness, mm		Theory	Experiment	Theory	Experiment	Theory	Experiment
Cold rolled	1.2	180	180	275	225	1800	1800
	1.6	340	340	170	170	1900	1900
Hot rolled	1.2	640	680	1580	1580	1900	1900
	1.6	340	340	1100	1100	1300	1300

orientations {100} grew out and developed. While away from the rolling direction precipitation of crystals with similar orientation {111} occurs. This would give rise to low dislocation density. Another plausible reason could be the greater presence of the second phase particles along the rolling directions than could be expected.

4.4 Degree of Deformation

The rearrangement and annihilation of the lattice defects result in the change of many physical properties. The measurement of these changes yields valuable information on the properties of defects. In a metal plastically deformed at low temperatures, a large number of defects are generated. If this metal is subjected to gradual heat-treatment the defects are activated at different temperatures, and their mutual annihilation decreases the internal energy of the crystal. X-ray investigations have shown that recrystallization begins at the same time as the rapid energy release. Naturally, the development of the recrystallization process depends upon the magnitude of the previous deformation. With very large internal stresses, the thermodynamic instability of the internal stresses occurs at lower temperature. Stored energy increases as degree of deformation increases while temperature of recrystallization decreases.

Table 4 shows that the degree of deformation decreases with sheet thickness in the rolling direction as well as at 90° to the rolling direction in hot rolled sheets. However, deformation increases with material thickness at 45°.

For cold rolled sheets, the degree of deformation decreases with sheet thickness at 45° to the direction of rolling. At 90°, the degree of deformation increases with sheet thickness. In the rolling direction as well as normal to this direction, the property of the test samples decreases as the thickness of the materials increases.

Plastic flow can be accommodated readily without imposition of extra external effort, which is related to low degree of deformation. Inhomogeneity in the distribution of phases and presence of gaseous pores and their positions could be the cause of this phenomenon.

Table 3 Values of dislocation density (k) for some 1xxx Aluminum sheets

		Dislocation density, mm^{-2}							
		Cold worked					Hot worked		
Sheet thickness, mm		0.7	0.9	1.0	1.2	1.6	1.1	1.2	1.6
Inclination to rolling direction	0°	10^6	10^6	10^6	10^7	10^7	10^7	10^7	10^7
	15°	10^6	10^6	10^6	10^6	10^6	10^6	10^6	10^6
	30°	10^5	10^5	10^5	10^5	10^5	10^5	10^5	10^6
	45°	10^4	10^4	10^4	10^4	10^4	10^5	10^5	10^5
	60°	10^3	10^4	10^4	10^4	10^4	10^4	10^4	10^5
	75°	10^3	10^4	10^4	10^4	10^4	10^4	10^4	10^4
	90°	10^2	10^3	10^3	10^4	10^4	10^4	10^4	10^4

Table 4 Values of degree of deformation (γ) for some 1xxx Aluminum sheets

		Degree of deformation							
		Cold worked					Hot worked		
Sheet thickness, mm		0.7	0.9	1.0	1.2	1.6	1.1	1.2	1.6
Inclination to rolling direction	0°	2.15	1.75	1.55	1.90	1.70	2.10	2.0	1.65
	15°	3.25	2.10	1.55	2.10	1.57	1.55	2.4	1.35
	30°	2.55	2.78	1.62	1.85	1.46	2.80	2.1	2.06
	45°	3.00	2.05	1.50	1.35	1.00	2.80	3.15	3.17
	60°	2.60	2.85	1.95	1.95	1.54	3.10	2.00	3.67
	75°	2.70	2.03	2.65	2.15	2.52	2.00	4.09	2.05
	90°	1.10	3.55	1.65	2.55	3.94	3.10	2.73	2.70

4.5 Effective Stress

Table 5 shows a comparison of effective stresses obtained experimentally with those derived from the model for the strain range $0 \leq \varepsilon \leq 0.6$ for hot and cold rolled sheets. The model and experimental results have good agreement in the rolling direction as well as direction normal to rolling direction. However, the result of experiment at 45° to the rolling direction is about half that of the model results in 1.2 and 1.6 mm hot rolled metals. Thus, the model over-estimates stress at 45° to the rolling direction. For cold rolled sheets, there is fairly good agreement between experiment and model results except at 90° in 1.2 mm sheet, where the model under-predicts the stress.

With the results of yield stress and effective stress for both experiment and model relation having close agreement, the developed analytical model can be used to study the anisotropic stress variation in aluminum sheets. It can also be used as a ready tool of the quality control department to determine whether there is homogeneous recovery after annealing of rolled sheets and the likely presence of residual stresses that could initiate corrosion whenever the material is in an aggressive environment.

5. Conclusion

Although significant developments in analysis and design capabilities have been achieved in modern technology, there still exists a gap between the simulation-based design and

Table 5 Variation of effective stress with inclination to rolling direction (strain, $0 \leq \varepsilon \leq 0.6$)

		Effective stress, MPa with inclination to the rolling direction					
		0°		45°		90°	
Sheet thickness, mm		Experiment	Model	Experiment	Model	Experiment	Model
Cold rolled	1.2	90	105	170	175	190	100
	1.6	160	125	170	170	170	190
Hot rolled	1.2	100	110	50	80	105	100
	1.6	120	120	90	180	100	110

manufacturing process. The problem of accurate numerical method that takes care of large deformation, while avoiding complicated constitutive relation, has been developed. A macro-mechanical property based model derived from the fundamental deflection equation of beam/column, has been used to make the stamping optimization process practical.

In the study, the deflection equation of beam/column has been used for the first time, to describe anisotropic plastic flow in sheet metals.

The degrees of deformation and dislocation density have been evaluated to determine the extent of microstructural inhomogeneity of the material and the level of recovery that has taken place. These phenomena can be investigated in deformed materials after rolling, before and after annealing, and also after the stamping operation.

References

1. F. Barlat, S. Panchanadeeswaran, and O. Richmond, Earing in Cup Drawing Face-Centered Cubic Single Crystals and Polycrystals, *Metall. Trans.*, 1991, **22A**, p 1525–1534
2. R. Becker, R.E. Smelser, and S. Panchanadeeswaran, Simulations of Earing in Aluminum Single Crystals and Polycrystals, *Model. Simul. Mater. Sci. Eng.*, 1993, **1**, p 203–224
3. K. Inal, P.D. Wu, and K.W. Neale, Simulation of Earing in Textured Aluminum Sheets, *Int. J. Plasticity*, 1999, **16**, p 635–648
4. R. Hill, A Theory of the Yielding and Plastic Flow of Anisotropic Metals, *Proc. Roy. Soc. London*, 1948, **193**, p 281–297
5. M. Gotoh, A Theory of Plastic Anisotropy Based on a Yield Function of Fourth Order (Plane Stress State), *Int. J. Mech. Sci.*, 1977, **19**, p 505
6. J.L. Bassani, Yield Characterization of Metals with Transversely Isotropic Plastic Properties, *Int. J. Mech. Sci.*, 1977, **19**, p 651
7. R.W. Logan and W.F. Hosford, Upper Bound Anisotropic Yield Locus Calculations Assuming <111>-Pencil Glide, *Int. J. Mech. Sci.*, 1980, **22**, p 419
8. F. Barlat and J. Lian, Plastic Behaviour and Stretchability of Sheet Metals I, A Yield Function for Orthotropic Sheet Under Plane Stress Conditions, *Int. J. Plasticity*, 1989, **5**, p 51
9. F. Barlat and D.J. Lege, A Six-Component Yield Functions for Planar Anisotropic Materials, *Int. J. Plasticity*, 1991, **7**, p 693
10. K. Chung and K. Shah, Finite Element Simulation of Sheet Metal Forming for Planar Anisotropic Metals, *Int. J. Plasticity*, 1992, **8**, p 453–476
11. V. Pegada, Y. Chun, and S. Santhanam, An Algorithm for Determining the Optimal Blank Shape for the Deep Drawing of Aluminum Cups, *J. Mater. Process. Technol.*, 2002, **125-126**, p 743–750